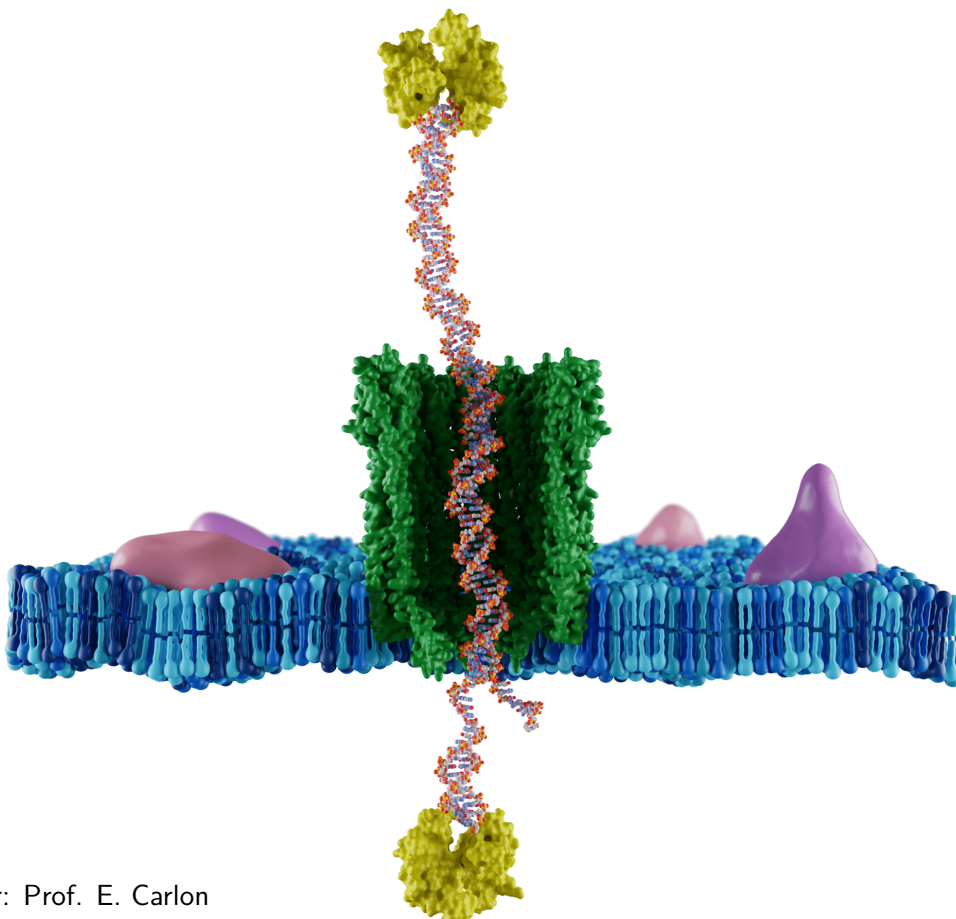


Coarse-grained simulations of the DNA nanopiston



Jan Stevens

Supervisor: Prof. E. Carlon

Thesis presented in
fulfillment of the requirements
for the degree of Master of Science
in Physics

Academic year 2020-2021

© Copyright by KU Leuven

Without written permission of the promoters and the authors it is forbidden to reproduce or adapt in any form or by any means any part of this publication. Requests for obtaining the right to reproduce or utilize parts of this publication should be addressed to KU Leuven, Faculteit Wetenschappen, Geel Huis, Kasteelpark Arenberg 11 bus 2100, 3001 Leuven (Heverlee), Telephone +32 16 32 14 01. A written permission of the promoter is also required to use the methods, products, schematics and programs described in this work for industrial or commercial use, and for submitting this publication in scientific contests.

Abstract

abstract

Vulgariserende Samenvatting

Summary in dutch.

asdf

Summary in Layman's Terms

Summary in english.

List of Figures

1.1	Flagella motor	2
1.2	This is a figure	4
1.3	This is a figure	5
1.4	This is a figure	6
1.5	caption nog maken	7
1.6	Example of an expanded model of a simple liquid (J L Finney, Ph.D thesis)[.]	10
1.7	This is a figure	13
2.1	This is a figure [.]	17
2.2	This is a figure	19
2.3	This is a figure	20
3.1	Structure of the OxDNA model with the different interactions. Figure was taken form []. (H.B. is hydrogen bond)	23
3.2	This is a figure [.]	25
3.3	write caption[.]	26
3.4	write caption[.]	28
4.1	asdf asdf asdf asdf asd fasdf fasdf asf asdfasdfa asdfasdf asfasf. asdf asdf asdf asdf asd fasdf fasdf asf asdfasdfa asdfasdfa asdfasdf asfasf. asdf asdf asdf asd fasdf fasdf asf asdfasdfa asdfasdfa asfasf.	33
4.2	write caption	34
4.3	write caption	34

List of Tables

Contents

Abstract	i
Vulgariserende Samenvatting	iii
Summary in Laymans's Terms	v
List of Figures	ix
List of Tables	xi
Contents	xiii
1 Introduction	1
1.1 Thesis outline	1
1.2 Biological Nanopores	3
1.3 Deoxyribonucleic acid (DNA)	7
1.4 Polymer Physics	8
1.5 Computer Simulations	10
2 The DNA Nanopiston	15
2.1 Rotaxane Formation	16
2.2 Operating principles	17
2.3 Coarse-grained simulations	19
3 Improving the Model	23
3.1 OxDNA	23
3.2 DNA Thermodynamics	24
3.3 Forward Flux sampling	27
3.4 Computational setup	29
4 Simulations of the Rotaxane	31
4.1 Mixed Rotaxane	31
4.2 Conformational Fluctuations of the Rotaxane	32
4.3 Toehold Displacement Reaction	32
5 Conclusions and Perspectives	35
5.1 Results & Conclusions	35
5.2 Future Perspectives	35
A 1D Confined Diffusion	37
Bibliography	38
Bibliography	39

CHAPTER 1

Introduction

...if we were to name the most powerful assumption of all, which leads one on and on in an attempt to understand life, it is that all things are made of atoms, and that everything that living things do can be understood in terms of the jigglings and wiggles of atoms.

— Richard P. Feynman, *The Feynman Lectures on Physics*²

1.1 Thesis outline

All organisms in nature tirelessly perform work, struggling against an ever increasing entropy. This work is collectively performed by a countless number of molecular machines, all contributing to their specific tasks.

Despite being so abundantly present in nature, fabricating synthetic molecular machines turns out to be a difficult task. One of the biggest hurdles in this process arises from their corresponding length-scale. Often times these machines are not larger than a few nanometres, making the typical energy associated with the bonds and distortions of their structure comparable to thermal energy fluctuations. As a result of these thermal fluctuations in their environment molecular machines naturally perform a stochastic motion that complicates their functioning. Extracting useful work from these freely tumbling structures is almost impossible. To overcome this limitation most synthetic molecular machines are embedded in a larger complex providing necessary stability.

This phenomenon is also observed in nature, for instance in the interfacing of protein complexes with the phospholipid bilayer of cells. A widely known example is the bacterial flagella motor, which provides an efficient way for bacteria to roll and tumble throughout their environment. Just like in electrical motors, the flagella consists of a stator and a rotor. The stator is anchored into the cell membrane, while the rotor is allowed to freely rotate. The work is produced by the flow of cations through the stator. Inducing changes in the

1. INTRODUCTION

electrostatic interactions between the two parts of the flagella generates a unidirectional motion.

Similarly to macroscopic engines, heat is produced during the operation of molecular machines. When the structure is not capable of dissipating this heat efficiently, an excessive build-up compromises its durability. To mitigate this problem, large and soft molecules are often used in the design of nanomachines. A logical choice is the use of polymers, which can effectively dissipate heat as a result of their flexibility. Due to the programmability of DNA, using the Watson-Crick interactions, the DNA polymer provides additional aptitude. This makes DNA a popular material in nanotechnology.

The central topic of this thesis is studying the DNA nanopiston (Bayoumi et al.[.]), a DNA based molecular machine embedded into a phospholipid membrane. This nanopiston can be characterised as an autonomous molecular machine, which turns over chemical fuel to continuously perform work. The aim of this complex is to perform selective transport of DNA through a membrane.

The operation cycle of previously designed DNA transporters requires a supporting external bias. However, this specific nanopiston operates also against an external bias. The physics driving this machine is entropy and will be discussed in detail in throughout this thesis.

In the first chapter a comprehensive introduction of important concepts regarding the DNA nanopiston is given. Having laid this theoretical foundation, the structure and operation cycle of the DNA nanopiston is discussed in chapter two. Next the computational model used in this thesis is presented in chapter three. In chapter four, the results of these simulations is discussed. Finally chapter five will offer a discussion of these results and recommendations for further research.

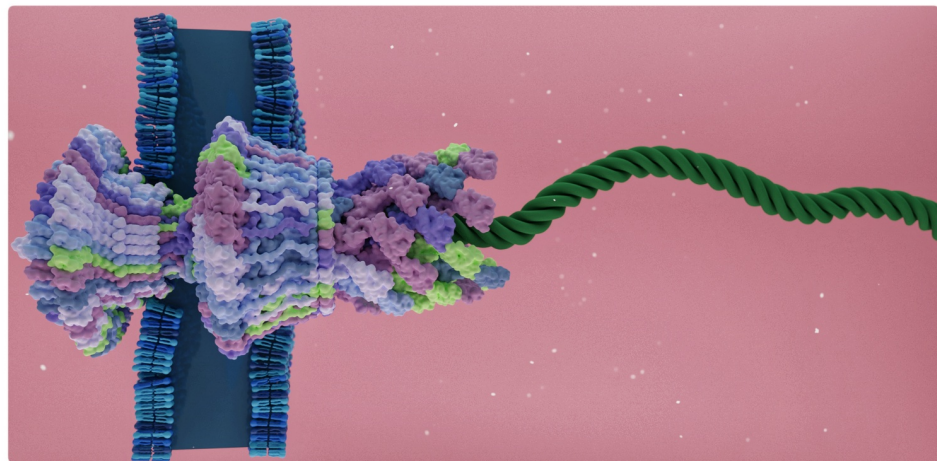


Figure 1.1: Flagella motor

1.2 Biological Nanopores

Biological nanopores are small perforations in a lipid bilayer membrane, created by a pore forming protein. The majority of these proteins are toxins produced by pathogenic bacteria. Their function in nature is to perforate the membrane of a cell, causing the cell to depolarize, disrupting vital cell functions. The perforation also induces an osmotic potential, causing cell nutrients to spill into the environment. Both effects eventually result in the killing of the cell.

The reason scientists are interested in studying nanopores is related to their size. These protein structures are generally only a few nanometres in diameter, making them comparable in size to the tiny transistors found in modern computers. Retrieving information from nano-scale processes has proven to be a challenging task. Developing sensors to probe this small length scale is thereby very relevant. This is the exact task nanopores provide a possible solution to, i.e. spectroscopy at the smallest scale.

Before delving into ionic current spectroscopy, the primary application of nanopores, a brief overview will be given of the structural properties of two popular biological nanopores.

1.2.1 α -Hemolysin (α -HL)

The α -Hemolysin (α -HL) protein is the most commonly used pore forming protein to create nanopores. It is produced by the *Staphylococcus aureus*, a bacterium commonly found in the human skin microbiome[.]

The α -HL pore (PDBID:7AHL[.]) is an oligomeric complex with multiple naturally occurring variations. The most typical configuration is a heptameric structure, meaning that there are seven protomers found in the complex. The secondary structure elements consist principally of β -sheets, making them a member of the β -barrel pore-forming toxins. Through both electrostatic and hydrophobic interactions, the α -HL is bound to the membrane of a target cell. Here the monomers assemble to a 'prepore' complex that transitions to the stable pore complex by inserting the β -barrel into the membrane[.]

Structurally the shape of α -HL resembles that of a hollow mushroom, see fig The total height of the complex is 11nm and the maximum width is measured to be 10nm. The internal chamber of the pore located at the cis-side of the membrane is called the lumen. The lumen of α -HL is quite constricted having a diameter of merely 3 nm. At the membrane the lumen chamber transitions into a protein stem, referred to as the constriction of the pore. Here the diameter of the chamber is reduced to a minimum of 1.5nm. On the wall of α -HL's inside chambers, the charges are relatively uniformly distributed. This will play an important role in further applications[.]

1. INTRODUCTION

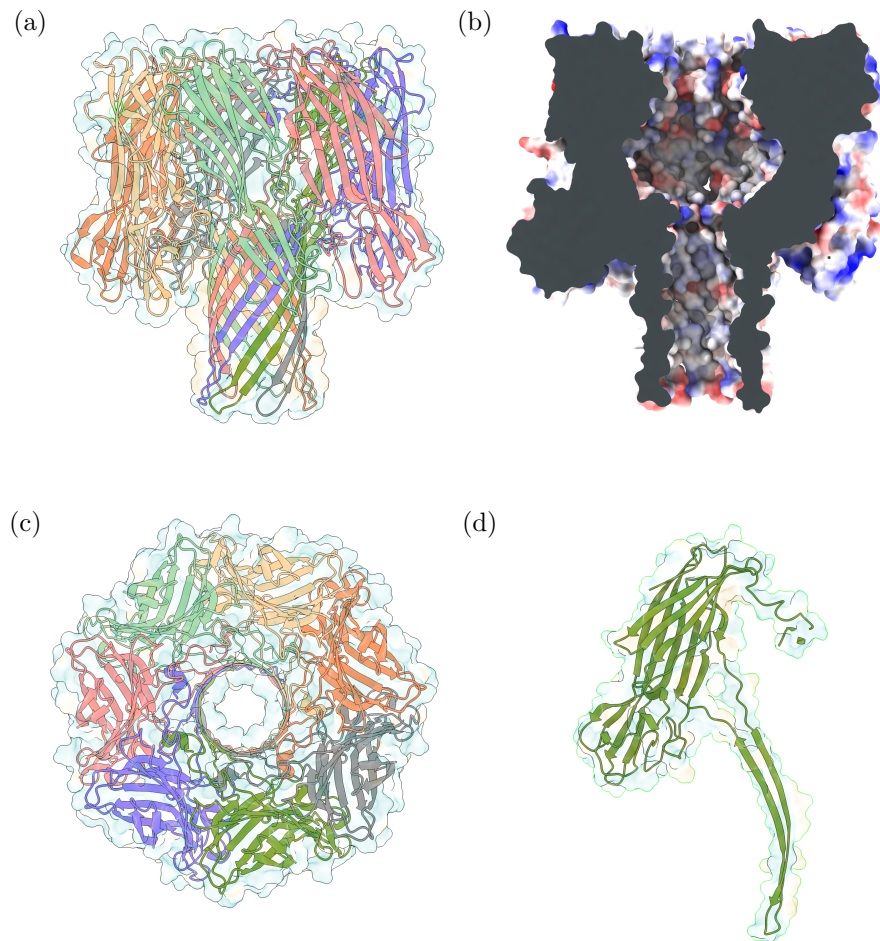


Figure 1.2: This is a figure

1.2.2 Cytolysin A (ClyA)

The Cytolysin A (ClyA) is a larger type of pore forming protein first found to be secreted by *E. coli* strains[.]. The larger size of its lumen allows for different types of applications compared to smaller complexes like α -HL. The larger diameter of the pore's stem allows for translocation of double stranded DNA, which is most relevant for this thesis.

The ClyA pore (PDBID:6MRT[.]) is an oligomeric complex most typically found in a dodecameric configuration, meaning that there are twelve protomers found in the complex. In nature small variations on this configuration are found. The secondary structure elements consist principally of α -helices, making it a member of the α -pore-forming toxins. The protein formation is induced by the hydrophobic interactions between the monomers β -hairpin and the solvent. The main structural rearrangement in this process consists of swinging out this β -tongue and inserting it into the membrane. After this transition, the membrane-bounded monomers oligomerize to form the final pore structure.

Structurally the shape of ClyA resembles that of two hollow cylinders stacked on top of each other. This cylinder approximation will be important later on in this thesis, where it will be used to create a simplified model of the nanopore. The total height of the complex is 14nm and the maximum width is measured to be 11nm. The lumen's size of this nanopore differentiates it from the previously discussed α -HL. The cis-entrance of the lumen measures 6nm, while the constricted side of the pore is still 3.6nm in diameter. In contrary to the α -HL, the inside surface of ClyA has a net negative charge, making it cation sensitive. This excess charge will induce significant coulomb interaction between the pore and negatively charged analytes[.].

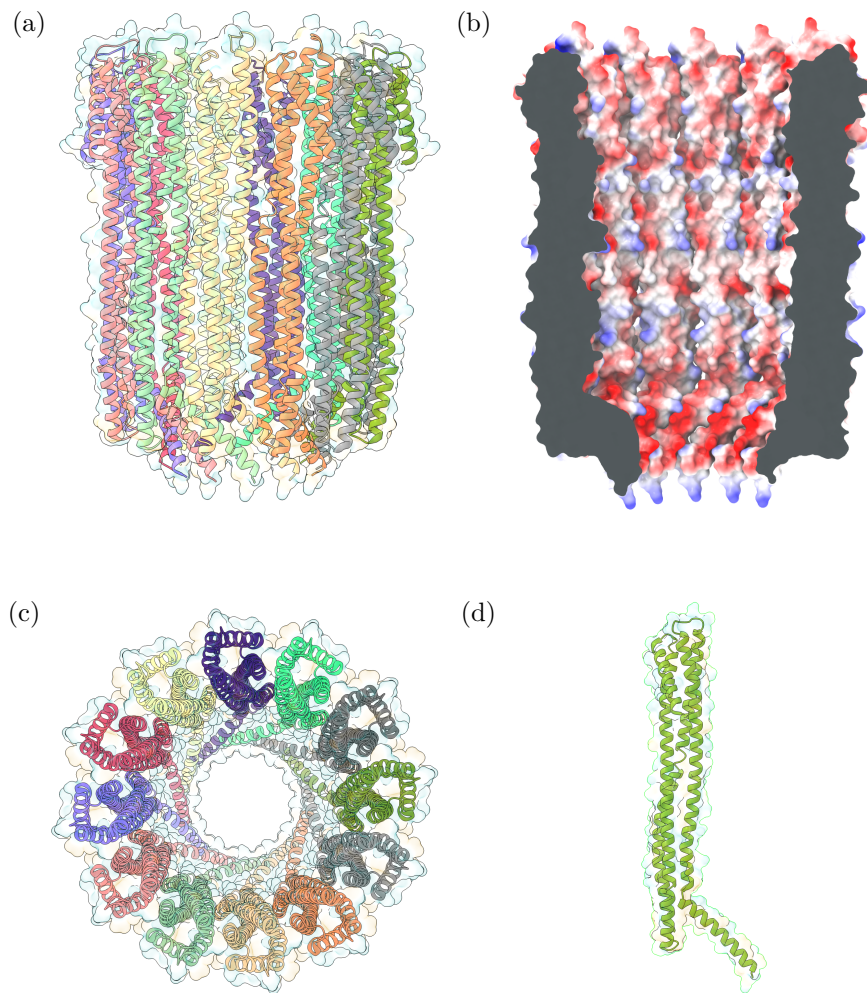


Figure 1.3: This is a figure

1.2.3 Ionic current spectroscopy

In recent years the study of nanopores became a popular research domain, mainly due to the development of the nanopore-based ionic current spectroscopy. For the case of biological nanopores, this method is depicted in figure 1.4. A lipid bilayer is perforated using a pore forming protein, for example α -HL. The membrane separates two compartments filled with a saline solution. When a potential difference is created over the membrane, the nanopore mediates an ion current between the two liquid-filled compartments.

This ion current through the pore can accurately be measured. If the pore is empty we refer to the measured current as the open-pore current. However, the applied electric field also induces forces upon analytes dissolved in the liquid. The net result of these interactions is a flux of analytes towards and in some cases through the nanopore. Analytes located inside of the nanopore partially block the ion current through the pore, reducing the measured current. Using machine learning algorithms the time series of these current fluctuation can be measured and identified with particular analytes in the solution. These methods are so precise that they allow for single cell spectroscopy.

It should be noted that besides these biological nanopores there are also inorganic nanopores in development[.]. An example are solid state nanopores created by making perforations in a semi-conductor wafer. While currently not as accessible as biological nanopores, mainly due to their high production costs, this method has some major advantages. First of all the material properties provide a chemical robustness not present in biological nanopores. The production process also allows for easy scalability and customisability. While currently not as widely used as biological nanopores, solid state nanopores will prove to be an important asset in the future of nanotechnology.

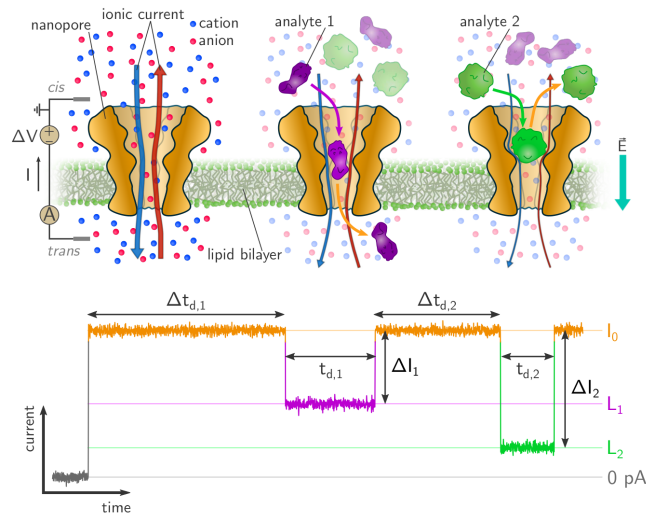


Figure 1.4: This is a figure

1.3 Deoxyribonucleic acid (DNA)

Deoxyribonucleic acid (DNA) is a long biopolymer composed of two strands, commonly found in its characteristic double helix structure. DNA is most famously known for storing the genetic code of organisms in the nucleus of their cells. The existence of this genetic code was already postulated by the Greek philosopher Aristotle. He developed a heredity theory based upon "blueprints", in which he tried to explain why physical traits were passed on from generation to generation[.]. This theory would go unnoticed until in 1869, when Friedrich Miescher discovered a new microscopic substance found on discarded surgical bandages. He would call this substance "Nuclein" since it originated from the nucleus of the cell.[.] Later it was found that this new substance, currently known as "Deoxyribonucleic acid", plays an important role as a blueprint for the perpetuation of living matter[.]

The structure of DNA was first determined by Rosalind Franklin using X-ray crystallography. Later this research was published by Watson and Crick, who concluded that DNA consists of two individual strands forming a double helical structure[.] Each strand is a chain of monomers, which we call nucleotides. A nucleotide is made up of a deoxyribose sugar, phosphate group and one of four nitrogenous bases: cytosine(C), guanine(G), adenine(A) or thymine(T). The covalent bonds that give both strands structure are formed between consecutive phosphate groups, which together make up the DNA backbone. To form the double helix, two backbones are held together by selective hydrogen bonds occurring between corresponding bases of opposing strands. These dipole interactions give rise to a selection rule, allowing to only form A-T and C-G base pairs.

Since the binding of the two strands is mediated by hydrogen bonding, association and dissociation is possible. The study of these processes is called DNA thermodynamics. The dissociation process of double stranded DNA (dsDNA) is called DNA melting, resulting in two individual strands of single stranded DNA (ssDNA). The reverse process is called DNA hybridisation, which is the selective binding of complementary nucleotides to form dsDNA.

The double helix structure of DNA comes in three different types, B-DNA, A-DNA and Z-DNA, all having a slightly different geometric arrangement. In nature the B-form is most commonly observed, which is characterised by a right-handed helix and the coplanarity between the complementary bases as shown in Fig. A helical twist of B-DNA consists of around 10 base pairs, having a net helical pitch of 0.34nm . During this thesis, when analysing DNA, we refer to the B-DNA form.

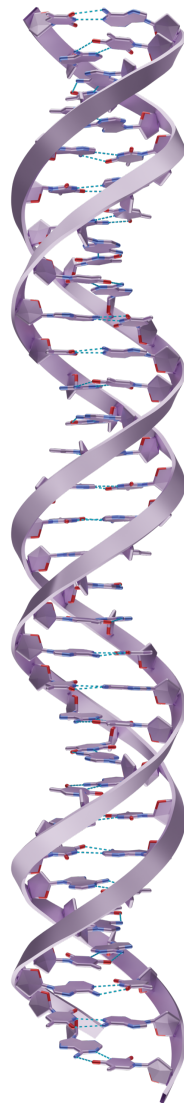


Figure 1.5: caption nog maken

When studying DNA the statistical theory of polymer physics is a useful tool. An atomistic resolution is not always needed to accurately describe processes involving relatively long DNA strands. Reducing the complexity of DNA to the monomer level is often justified, allowing us to use more general results in polymer physics.

1.4 Polymer Physics

A polymer is a biomolecule made up of building blocks called monomers, linked together to form a chain. The configuration of this chain is determined by the position vector of each monomer, denoted as $\{\mathbf{r}_0, \mathbf{r}_1, \dots, \mathbf{r}_N\}$. The link between each consecutive pair of monomers is called the bond-vector, defined as $\mathbf{u}_i = \mathbf{r}_i - \mathbf{r}_{i-1}$. During this discussion we will assume these bonds to be inextensible, i.e. having a fixed bond length of $|\mathbf{u}_i| = a$.

Various different models can be used to describe a polymer. The most simple version is called the Freely Jointed Chain (FJC). This model is an example of an ideal flexible polymer, in which excluded volume interactions or polymer bending rigidity are not taken into account. In this model, it is assumed that each bond-vector is completely uncorrelated with its adjacent bonds. Mathematically this is represented by assigning the bond-vector orientation an uniform probability distribution

$$g(\mathbf{u}) = \frac{1}{4\pi a} \delta(|\mathbf{u}| - a), \quad (1.1)$$

where a is the fixed bond length.

The above described model provides a relatively accurate description of long polymers. However, the assumption that consecutive monomers are uncorrelated becomes problematic at small length scales. The Kratky-Porod model, or discrete wormlike chain, solves this problem by taking the energetic cost of bending the polymer into account. Mathematically this is done introducing a bending rigidity between neighbouring bonds in the form of a coupling constant, $\kappa > 0$. Each polymer configuration is assigned an energy using the equation,

$$E_{WLC} = -\kappa \sum_{i=1}^N \hat{\mathbf{u}}_i \cdot \hat{\mathbf{u}}_{i+1} = -\kappa \sum_{i=1}^N \cos \theta_i, \quad (1.2)$$

where $\hat{\mathbf{u}} = \mathbf{u}/a$ is the unit bond-vector and θ_i is the angle between neighbouring bond-vectors $\hat{\mathbf{u}}_i$ and $\hat{\mathbf{u}}_{i+1}$. The lowest energy state of this discrete wormlike chain is a straight rodlike configuration, where the bond angles θ_i are minimized.

To calculate the bond-vector correlation function, we first determine the partition function, Z_{WLC} , of the system. Identifying the single monomer contributions, this quantity factorises

into a product of single bond-vector partition functions as

$$\begin{aligned} Z_{\text{WLC}}(N, T) &= \int_0^\pi \cdots \int_0^\pi d\theta_1 \dots d\theta_N \sin \theta_1 \dots \sin \theta_N e^{\beta \kappa \sum_{i=1}^{N-1} \cos \theta_i} \\ &= \left[\int_0^\pi d\theta \sin \theta e^{\beta \kappa \cos \theta} \right]^N \\ &= [Z_{\text{WLC}}(1, T)]^N, \end{aligned} \quad (1.3)$$

where $\beta = 1/\kappa_b T$ is the inverse temperature. It rests us to determine the single bond-vector partition function. Carrying out the integration yields the result,

$$Z_{\text{WLC}}(1, T) = \int_0^\pi d\theta e^{\beta \kappa \theta} = \frac{2 \sinh(\beta \kappa)}{\beta \kappa}. \quad (1.4)$$

From the found partition function we can now determine the bond-vector correlation function. Using the definition of the partition function, we determine the average cosine of the angle between consecutive bonds to be,

$$\begin{aligned} \langle \cos \theta_{i+1} \rangle &= \frac{\partial \log Z_{\text{WLC}}(1, T)}{\partial (\beta \kappa)} \\ &= \frac{1}{\tanh(\beta \kappa)} - \frac{1}{\beta \kappa}. \end{aligned} \quad (1.5)$$

Studying the conformation of polymers is often times done assuming a low temperature or large bending rigidity, where we find that the above expression simplifies. In the limit, $\beta \kappa \gg 1$, the lowest order approximation yields,

$$\langle \cos \theta \rangle \approx 1 - \frac{1}{\beta \kappa}. \quad (1.6)$$

Decomposing the bond-vector $\hat{\mathbf{u}}_{n+1}$ in terms of an orthonormal basis, defined by the normal and tangential directions of the preceding vector $\hat{\mathbf{u}}_n$, gives

$$\hat{\mathbf{u}}_{n+1} = \hat{\mathbf{u}}_n \cos \theta_n + \hat{\mathbf{u}}_n^\perp \sin \theta_n. \quad (1.7)$$

This decomposition allows us to express the correlation between distant bond-vectors in terms of the correlation between neighbouring bonds-vectors. The factorisation yields

$$\langle \hat{\mathbf{u}}_i \cdot \hat{\mathbf{u}}_{i+m} \rangle = \langle \hat{\mathbf{u}}_i \cdot \hat{\mathbf{u}}_{i+m-1} \rangle \langle \cos \theta \rangle = \dots = \langle \cos \theta \rangle^m, \quad (1.8)$$

where we used the fact that the sinusoidal terms vanish due to symmetry. Exploring this result in the limit, $\beta \kappa \gg 1$, we find the expression

$$\langle \hat{\mathbf{u}}_i \cdot \hat{\mathbf{u}}_{i+m} \rangle = e^{m \log(1 - \frac{1}{\beta \kappa})} \approx e^{-na/l_p}, \quad (1.9)$$

introducing a new polymer quantity, the bending persistence length

$$l_b \equiv \frac{a \kappa}{k_b T}. \quad (1.10)$$

This general result in polymer physics states that the correlations between bond-vectors is exponentially decreasing. The defined quantity represents the characteristic length scale of the polymer, over which the correlations between bond-vectors is lost.

Two limiting cases can be explored. Firstly, in the case where the persistence length is much larger than the polymer's length, $l_p \gg na$, all bond-vectors are correlated, i.e. the polymer approximates a straight rod. For the reverse case, where $l_p \ll na$, it can easily be shown that the polymer behaves as a stochastic walk.

The persistence length is a central result in the theory of polymer physics, providing a measurable quantity related to the bending rigidity of a polymer. During the simulations performed in this thesis, the notion of bending persistence length is used to discuss the flexibility of the DNA polymer.

1.5 Computer Simulations

The theory of classical mechanics is often regarded as the first major breakthrough in the field of physics. For every aspiring physicist this is still the starting point of their studies. Unfortunately, getting to know these relatively simple laws of nature leads to the inescapable realisation that these theories are expressed in mathematical formalisms that are only analytically solvable in few idealised scenarios. Applying these formulas to a problem consisting of just more than two particles already leads to practically unsolvable equations.

Although it is often not possible to find an exact solution to equations related to complex physical systems, finding reasonable approximations to their solution is achievable. One popular method to analyse the dynamics of complex systems is the use of simulations.

Simulations have a rich history within physics and engineering, starting even before the invention of the computer. An example of one of these mechanical simulations is the 'Waterloopkundig Laboratorium', a hydrological laboratory located in Delft[.]. This laboratory houses a scale model of important Dutch waterways, where the influence of waves on harbours and docks was studied. The simulation provided revolutionary insights into the behaviour of water and played an important part in the design of the famous Delta Works.

Another more topical example is the use of mechanical simulations to study the structure of water. In the early 20th century Prof. J.D. Bernal and his fellow researchers build various ball and stick models of water to

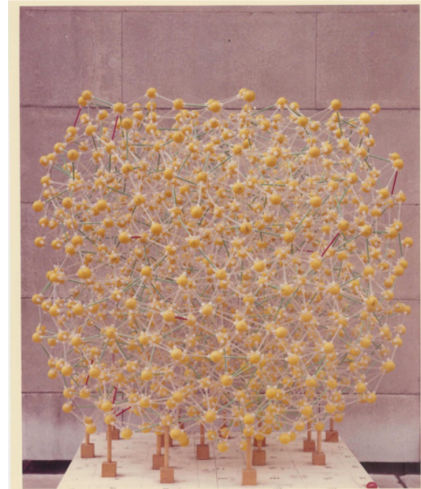


Figure 1.6: Example of an expanded model of a simple liquid (J L Finney, Ph.D thesis)[.]

analyse the possible 3D configurations of water molecules in a liquid[.]. Their research eventually explained the peculiar physical properties of water from an atomistic perspective. Despite how useful these mechanical simulations turned out to be, the biggest drawback of the method was the extreme cost of labour involved with their construct. As Prof. Bernal alluded to in his famous 1962 lecture,

...I took a number of rubber balls and stuck them together with rods of a selection of different lengths ranging from 2.75 to 4 inch. I tried to do this in the first place as casually as possible, working in my own office being interrupted every five minutes or so and not remembering what I had done before the interruption...[.]

After the first computer simulations were performed in the Los Alamos laboratory[.], the popularity of simulations rapidly increased. The remarkable explanatory power of simulations, combined with the relative easy construction of computer models, led to a fast adoption of computer simulations in the scientific community. Within the context of this thesis, computer simulations are used to study the mechanics of the DNA polymer. Due to the high number of atoms in a typical system it is generally not possible to find an analytical solution to their equations of motion. In this context simulations are often used to gain an insight into the complex dynamics of the system and guide the developments of more simple approximate theories. The simulations act as a bridge between the microscopic constituents of the systems and the macroscopic properties we want to understand.

1.5.1 Molecular Dynamics Simulations

Molecular Dynamics (MD) is a computer simulation technique, used to analyse the dynamics of a classical many-body system. The central idea of this method is to generate all the trajectories in a system of N particles by numerically integrating the classical equations of motion,

$$m_i \frac{d^2 \mathbf{r}_i}{dt^2} = \mathbf{f}_i, \quad \mathbf{f}_i = -\frac{\partial}{\partial \mathbf{r}_i} \mathcal{U}_i, \quad \text{for } i \in N.$$

The motion of the particles are governed by the forces f_i acting upon them, which are usually derived from the interaction potentials U_i . Solving these differential equations is achieved by employing a discretized time integration scheme. Algorithm 1 shows the typical structure of a molecular dynamics simulation. The discretization resolution is conventionally called the time step of the simulations denoted by Δt .

There are a large number of different integrations schemes that one can choose from, in which the choice depends entirely on the system at hand. When working with an isolated system – i.e. microcanonical ensemble –, logically an energy conserving integrator is needed. The canonical choice for this type of integration scheme is the Velocity-Verlet algorithm. This algorithm is an example of leapfrog integration, where the updating of the positions and velocities are interleaved at different points in time. The major strength of this type of

algorithm is that it turns out to be a symplectic integrator. This means that the errors on the conserved energy are bounded.

On the other hand, when a system is in contact with a thermal reservoir –i.e. canonical ensemble– not the total energy is conserved, but rather the temperature of the simulation is fixed. To achieve this a thermostat is implemented in the MD simulation. A typical thermostat attempts to negate any drift in temperature by appropriately importing or exporting energy to the system after each time step. Popular examples of thermostats are the Nosé-Hoover thermostat or the Langevin thermostat. The latter regulates the temperature by introducing an implicit solvent to the simulation that gives rise to random thermal kicks. The resulting equations of motion are the Langevin equations given by,

$$m_i \frac{d^2\mathbf{r}_i}{dt^2} = -\nabla\mathcal{U}_i - \gamma_i \frac{d\mathbf{r}_i}{dt} + \xi_i(t), \quad (1.11)$$

where γ_i is known as the friction coefficient and $\xi_i(t)$ a stochastic force acting upon the particles. The combination of the last two terms fully capture the statistical consequences of the solvent interacting with the system.

Algorithm 1: The Velocity Verlet algorithm: *Nog maken*

Input : Configuration of the system at $t = 0$

```

1 newList = []
2 /* For odd elements in the list, we add 1, and for even
   elements, we add 2. */
3 for i ← 0 to n − 1 do
4   if isOddNumber(ai) then
5     | newList.append(ai + 1)      // Some thought-provoking comment.
6   else
7     | // Another comment
8     | newList.append(ai + 2)
9   end if
10 end for
11 return newList

```

1.5.2 Coarse Grained modelling

As most things do, molecular dynamics simulations have their pitfalls. A commonly encountered problem is the rapidly increasing computational cost when the number of particles in the system increase. If not addressed, this would limit the scope of MD simulations to systems of a few particles over short time-scales.

During these simulations the most costly calculations involve the non-bonded interactions in the system. These interatomic interactions make the computational complexity for rudimentary MD simulations scale as $O(N^2t)$, where N is the number of particles in the

system and t the simulation time. This bad scaling behaviour comes arises from the fact that for each individual particle all the other particles are contributing to its energy potential. To improve this scaling behaviour, the non-bonded interactions in a MD simulation are almost always truncated. This localization of the interatomic interactions has the favourable effect that not all atoms are involved in every calculation. Efficient algorithms, like the multigrid method, have been derived to improve the scaling complexity of MD simulations up to $O(Nt)$.[.]

Coarse graining is a method to further optimize molecular dynamics simulations. In all atom simulations each atom is explicitly represented as a particle in the simulation. Contrarily, coarse grained simulation use multiple atoms grouped together to form generalised pseudo-atoms, with their respective pseudo-interaction.

There are two distinctly different ways to construct a coarse grained model. The first method starts from the all atom model of the system and generalises nearby atoms into larger pseudo-atoms. This is called the bottom up approach. The top down approach, which is the alternative method, focuses more on the precise reproduction of experimental results. Here larger pseudo-atoms are designed based upon characteristic patterns in the structure. Next the pseudo-interactions are tweaked to accurately reproduce the system's dynamics.

In the field of DNA simulations coarse graining turned out to be a very important method. Previously all atom simulations of DNA polymers were restricted to simulations of less than hundred basepairs over only a few microseconds. The development of coarse-grained models allowed for the simulation of large scale systems, often encountered in DNA technology. A few examples of commonly used coarse grained models of DNA are Martini[.], 3SPN[.] and oxDNA[.].

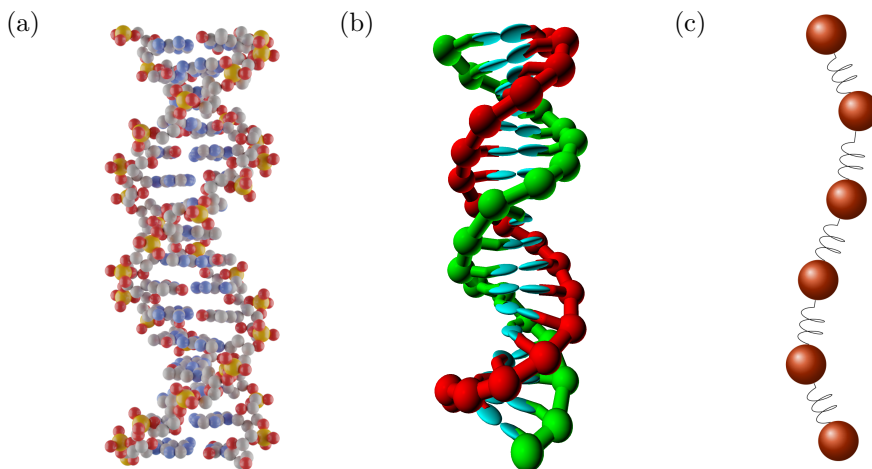


Figure 1.7: This is a figure

CHAPTER 2

The DNA Nanopiston

Chapter Reference

The contents of the chapter is based on:

- Bayoumi, M., Nomidis, S. K., Willems, K., Carlon, E., and Maglia, G. (2021). Autonomous and active transport operated by an entropic dna piston. *Nano Letters*, 21(1):762768. PMID: 33342212.

The central topic of this is the DNA nanopiston, a molecular machine developed by the Maglia research group[.]. The piston operates by turning over chemical fuel, consisting of ssDNA, into autonomous motion.

The design is based upon their earlier work, where the group developed a protein rotaxane[,], consisting of a polypeptide thread trapped in a Cya nanopore by two stopper proteins. This rotaxane could be moved between two stable states inside the nanopore by an electric potential, acting as a molecular switch.

This research lead to the development of the DNA nanopiston by Bayoumi et al.[.] in the Maglia group. In this new molecular machine the rotaxane now constitutes of a DNA strand instead of a polypeptide thread. Utilising the thermodynamic transitions of DNA, this complex is capable of actively transporting DNA cargo-strands through the nanopore.

In this chapter the work of Bayoumi et al. is discussed, giving an overview of the construction and operating cycle of this molecular machine. At the end of this chapter the molecular dynamics simulations from the paper of Bayoumi et al. are discussed, as they were the main inspiration behind our project.

2.1 Rotaxane Formation

Synthetic molecular machines are often times embedded in larger complexes, providing the necessary structure for their operation. For this reason biological nanopores are an suitable starting point in the development of molecular machines. These transmembrane proteins spontaneously self-assemble into well defined structures, embedded into a lipid bilayer. Extensive research has been performed, designing methods and tools to tailor their structural and electrostatic properties for specific use cases, originally focused on Ionic current spectroscopy. This large back catalogue of research can now be employed into building out their utility as an ideal building block for membrane bound molecular machines.

The design of the DNA nanopiston is centred around the biological nanopore Cytolysin A (ClyA). A modified variant ClyA-AS is used, which has been specially engineered for use in Ionic Current Spectroscopy[.]

The nanopore is used to anchor a DNA Rotaxane structure inside the lipid membrane. The large diameter of both its lumen and stem allows for the translocation of double stranded DNA through the pore.

3. The DNA complex, built from three ssDNA sequences: ssDNA 1, ssDNA 2, and ssDNA 3. The last 70 bases of ssDNA 2 are complementary to the first 70 bases of ssDNA 1, hence a complex with neutravidin on one end, a 70-base dsDNA and two ssDNA overhangs on the other end is formed, toehold. This complex is called the rotaxane.

2. The rotaxane is trapped in the nanopore by connecting it to two neutravidin stoppers via biotin

The initial configuration is inspired by Ionic current spectroscopy. A cya nanopore embeded on a lipid bilayer, seperating a saline liquid filed basin into two compartments.

To form the nanopiston Neutravidin (0.5 M), ssDNA1 (5-biotinylated, 100 bases, 1.2 M) and ssDNA 2 (80 bases, 1 M) were added to the cis solution. Applied a voltage of +100mV, equal to a downward force on the analytes. The applied voltage induces an open pore current through the pore, when the analytes enter the pore this blockage is measured. The complex is trapped inside to pore indefinitely until the voltage is reversed.

While keeping the potential at +100 mV, the addition to the trans side of neutravidin (1 M) and ssDNA 3 (3-biotinylated, 20 bases, 2 M), complementary to the last ten bases of the ssDNA 1 overhang of the trapped thread. With the aim of reducing the free enrgy in the system, the ssDNA strand hybridises will spontaneously hybridise with the other strand. The completion of the hybridisation is checked by reversing the potential over the pore, if the measured bloackage current remains the same it is assumed that the hybridisation has occurred and the rotaxane is formed.

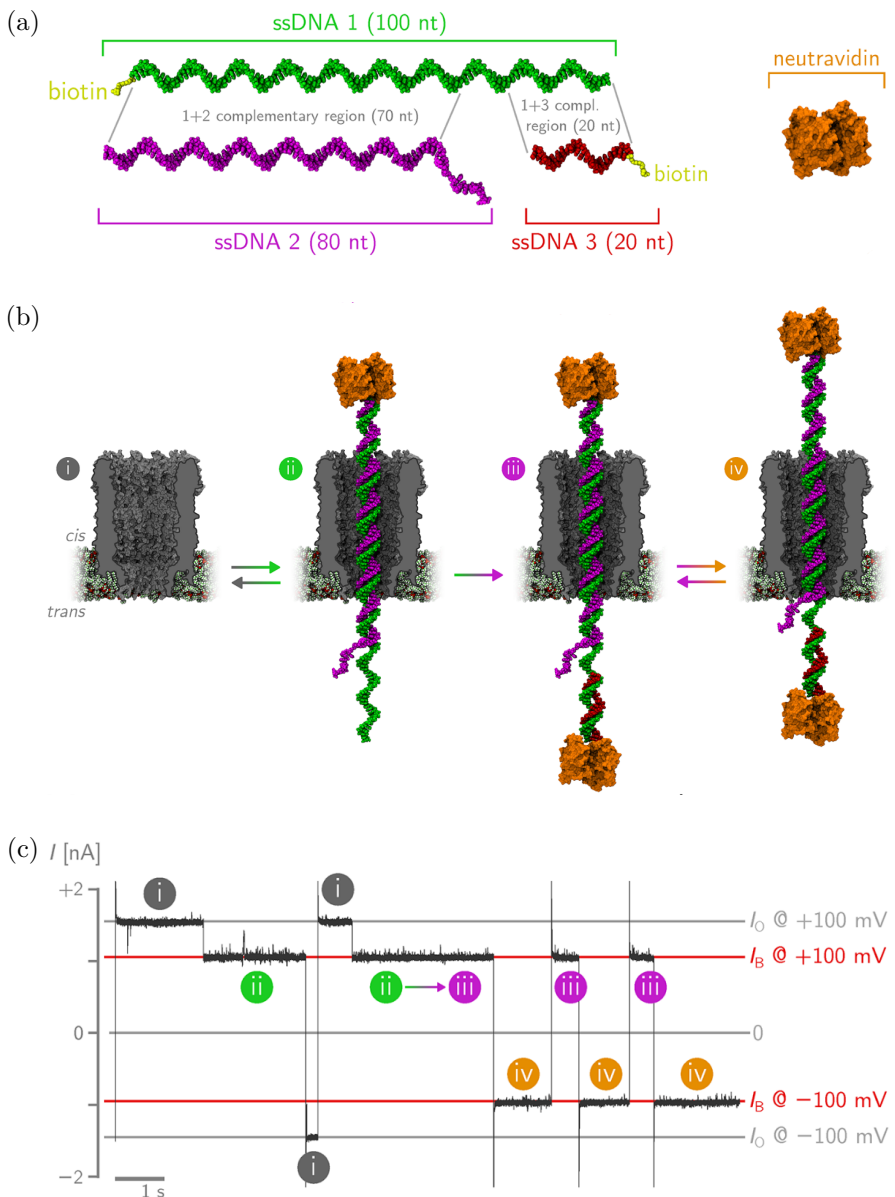


Figure 2.1: This is a figure [.]

2.2 Operating principles

Once rotaxane-ds is formed, the addition of ssDNA 4 (0.5M) to the trans chamber, which is fully complementary to ssDNA 2, induces the displacement of the latter in trans via a strand displacement reaction, using the ssDNA 2 overhang as a toehold (Figure 2)

During the strand displacement reaction, two possible transient states possibly occur.

2. THE DNA NANOPISTON

the cis neutravidin is transiently pushed toward the trans side, most likely entering the lumen of the nanopore (see Section S3).

The intermediate state of the strand displacement reaction can occur in two possible ways. In the first scenario, the DNA cargo is hybridized with the fuel exclusively outside the nanopore in the trans solution. This implies that neutravidin will enter inside the lumen of the nanopore. Indeed, previous studies have shown that avidin can enter the cis lumen of ClyA but cannot translocate through the nanopore. Alternatively, the strand displacement reaction can take place inside the nanopore. In this case, the DNA transport would occur from trans-to-cis rather than from cis-to-trans, as described in the main text. We think this is unlikely, because this scenario would require the translocation through the trans entry of three DNA strands

After the removal of ssDNA 2, a new configuration is obtained, in which ssDNA1 and ssDNA3 remain trapped within the pore. This configuration consists of a 90-base-ssDNA thread on the cis end, a 10-basepair-dsDNA stretch on the trans side, and neutravidin on both sides of the pore (Figure 2). We refer to this configuration as rotaxane-ss.

The subsequent addition of 0.5 M of ssDNA 2 cargo to the cis side restores rotaxane-ds, as ssDNA 2 hybridizes with the thread of rotaxane-ss

After each cycle, one cargo molecule is transported from cis to trans and one fuel molecule is expended.

These cycles were found to be both at positive, + 20 mV (Figure 2a, top trace), + 50 mV and +100 mV (Figure S3), and negative, - 20 mV (Figure 2a, bottom trace), biases. Higher negative applied potentials (e.g., 50 mV, Figure S3) prevented the cycling

The working of the nanopiston against and with external bias is important, postulated that it is due to the entropic interaction between the rotaxane and the pore. Discuss the importance of entropy. power stroke is toehold disp reaction. Results in two entropy state. This entropic energy provides the recovery stroke. Next hybridisation with the fuel strand makes us come back to the initial configuration.

Furthermore, the cycles were faster at positive than at negative applied potentials, but were slower as the potential was increased. This voltage dependency can be explained by toehold sequestering inside the nanopore

Due to brownian motion both autonomous and non-autonomous systems use ratcheting to eventually deliver work. Using this method minimal synthetic machines can deliver elegance and performance shedding the 'baggage' of biological evolution.

Figure 2.2a shows the measured current over through the nanopore during the operation cycle. The ionic current of rotaxane-ss is lower than the blocked current of rotaxane-ds most likely reflecting the coiled structure of ssDNA inside the nanopore. Shows the limitation of the experimental analysis of the pore, only view into the system is through the measured current. To get a more in-depth understanding of the conformal fluctuations of the pore computation analysis was performed in the form of molecular dynamics simulations.

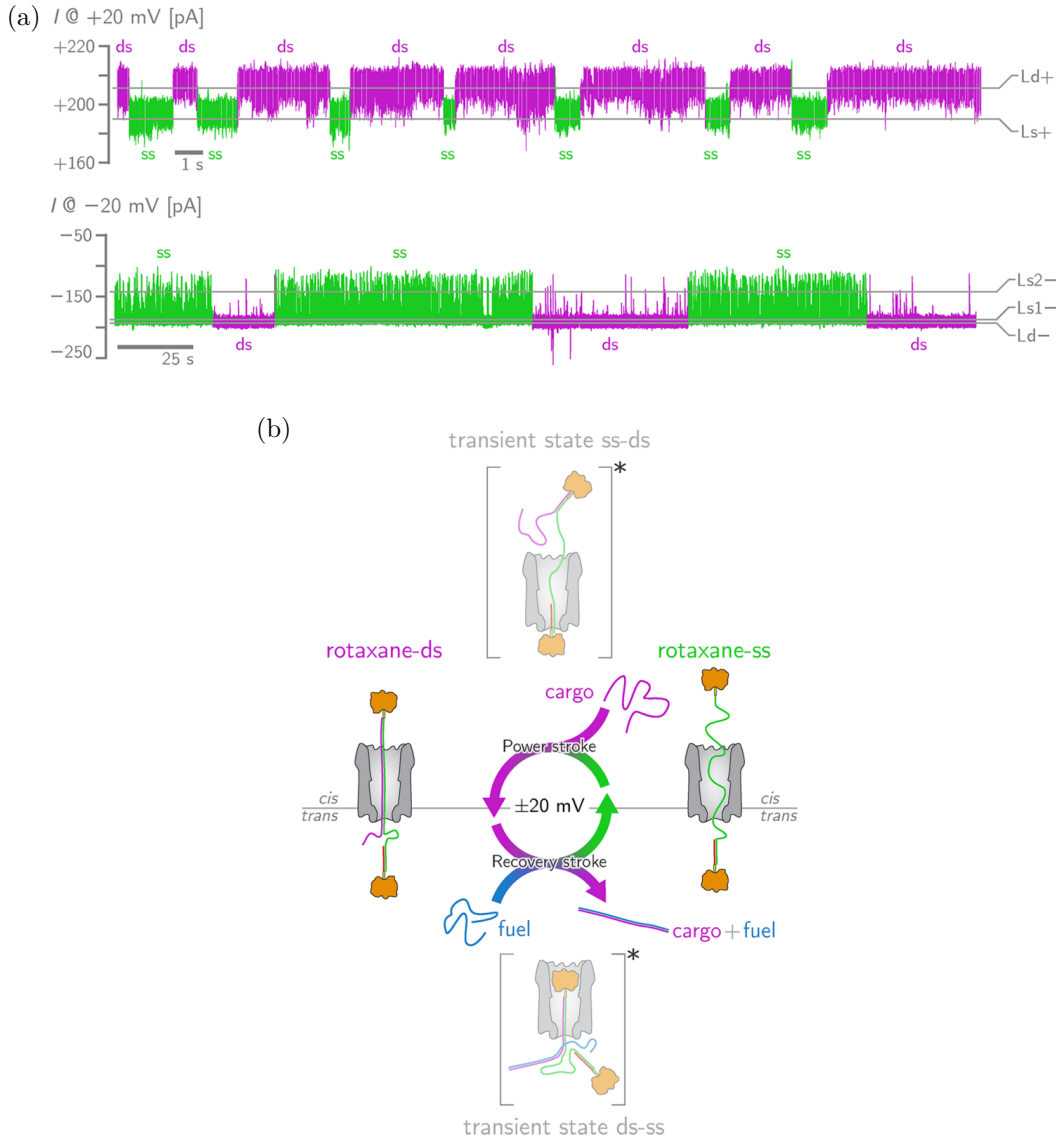


Figure 2.2: This is a figure

2.3 Coarse-grained simulations

to investigate the typical conformations of rotaxanes-ds and ss at zero bias. This approach is justified by the long time scales of interest, and the high salt concentration of the solution (2 M KCl). A numerical analysis of the electrostatic energies, using the Poisson-Boltzmann equations, indeed indicates that electrostatic DNA-nanopore interactions are weak and repulsive (Figures S4 and S5 in Section S8). These interactions were accounted for by properly adjusting the dimensions of the pore

2. THE DNA NANOPISTON

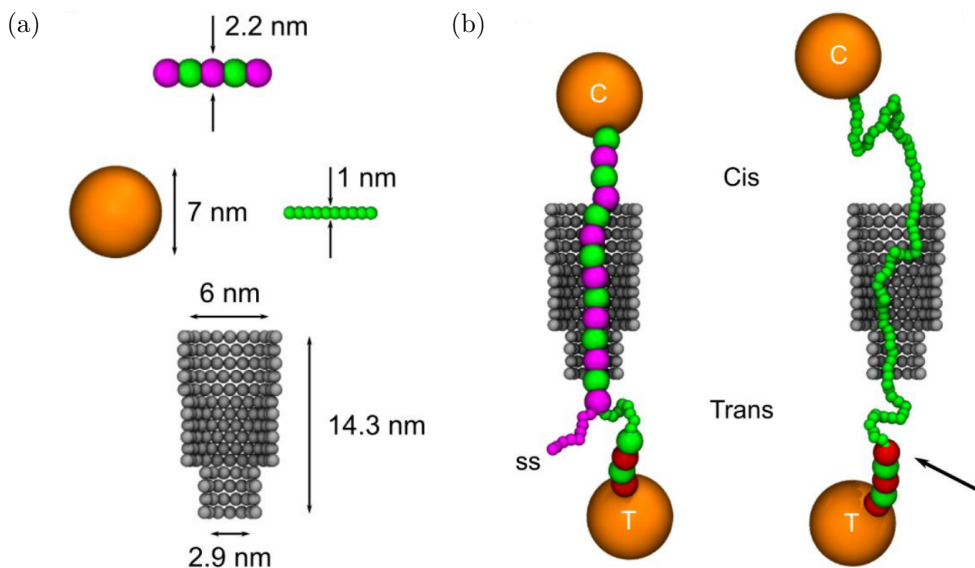


Figure 2.3: This is a figure

the fact that the piston operates at both positive and negative applied bias suggests that the electrophoretic bias is not necessary for its functioning. Indeed, simulations indicate that entropy plays a more central role.

LAMMPS.

Discuss semiflexible bead-and-spring model DNA + repulsive LJ interactions to simulate excluded volume interactions.

Each spherical ssDNA (dsDNA) bead represented 1 nt (ssDNA) or 5 bp (dsDNA), had a diameter of 1 nm (ssDNA) or 2.2 nm (dsDNA) and an average bond distance of 0.68 nm (ssDNA) or 1.7 nm (dsDNA).

ClyA consisted of three connected open cylinders, with diameters 6 nm, 5.5 nm and 2.9 nm from the cis- to the trans-side, following the geometry reported in [1]. The latter value is somewhat smaller than the reported one (3.3 nm), accounting for the electrostatic repulsion between DNA and the negatively-charged trans-entry. The lipid bi layer in which the pore is embedded is simulated by a reflective boundary at the lower entrance of the nanopore interacting only with the neutravidin beads.

Neutravidin was modeled as a sphere of diameter 7 nm, attached to the two ends of the rotaxane. The motivation of this size was done by simulating the neutravidin bead together with the ClyA nanopore and fitting the size of the neutravidin bead so that it could be captured in the lumen of the nanopore, as is seen in experiments.

The bond strength is chosen to be, by transforming the equation for persistence length $k_{\text{SsDNA}} = \text{persistence}_{\text{SsDNA}} * \text{boltzmann} * \text{temperature} / \text{length}_{\text{Nt}} k_{\text{DsDNA}} = \text{persistence}_{\text{DsDNA}} * \text{boltzmann} * \text{temperature} / \text{length}_{\text{Nt}}$

tenceDsDNA * boltzmann * temperature / lengthBp For the description of ssDNA and dsDNA, with persistence lengths 2.2 nm and 45 nm, respectively.

$$k_{bond} = l_p * k_{bt} * T / \langle a \rangle$$
 Kuhn segments for ssDNA en dsDNA are different!

Gaussian probably distribution of the beads, i.e. the beads show ideal chain behaviour.
Equipartition theorem.

$$k_{bond} = 3k_bT / \langle a \rangle$$

Langevin integrator is used As is common in simulations of coarse-grained models. As is common practice in MD simulations, the diffusion coefficient of the oxDNA strand is chosen larger then the value of physical DNA. This is done to speed up the simulations, while ensuring its physical accuracy.

Discuss limits of the model. Limited accuracy of the CG model since it does not caputre the full structure of DNA accurately. For example the double helix structure is note captured. Another consequence is that the DNA hybridisation can not be simulated using this model, since both ssDNA nucleotides and dsDNA basepairs are represented by simple beads. To further analyse and understand the operation cycle of the nanopiston a more accurate CG model is needed.

3

CHAPTER

Improving the Model

All models are wrong, but some are useful.

— George Box

3.1 OxDNA

OxDNA is a coarse-grained model of DNA developed by Thomas E. Ouldridge et al. at the University of Oxford. The central aim of the project was to develop a coarse-grained model of DNA, that could be used in the design of DNA technology. For the development of these technologies a model was needed that accurately captured the structural, mechanical and thermodynamical properties of DNA, while keeping the computational cost low.

The OxDNA model represents each nucleotide in the DNA strand as a rigid unit. Each rigid nucleotide has three independent interaction sites, each capturing a different aspect of the model. The interactions between these pseudo-atoms are compared to experimental data to calibrate the interactions, characterising their approach as "top down" coarse-graining. The interactions defined in the OxDNA model can be summarized as,

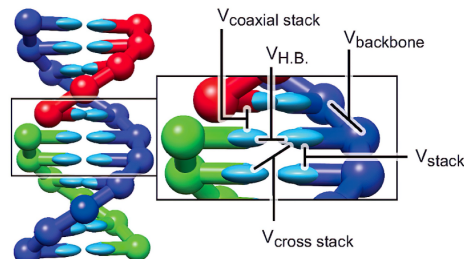


Figure 3.1: Structure of the OxDNA model with the different interactions. Figure was taken from [1]. (H.B. is hydrogen bond)

3. IMPROVING THE MODEL

$$V = \sum_{\text{nearest neighbours}} \left[V_{\text{backbone}} + V_{\text{stack}} + V'_{\text{exc}} \right] \\ + \sum_{\text{other pairs}} \left[V_{\text{H.B.}} + V_{\text{cross stacking}} + V_{\text{exc}} + V_{\text{coax stack}} \right]. \quad (3.1)$$

The first interaction site is the hydrogen-bonding/base excluded volume site, incorporating the hybridisation of complementary nucleotides into the model. The hydrogen-bonding interactions are not fixed, allowing for OxDNA to simulate dsDNA, ssDNA and their thermodynamic transitions.

The second is an excluded volume interaction site located at the backbone. This site's main role is to simulate the covalent bonding between consecutive phosphate groups. These permanent bonds provide structure to the ssDNA strands by forming the backbone.

The last interaction site is again located at the base, where it provides a base stacking interaction between consecutive nucleotides. The nucleotide stacking in DNA is crucial for the formation of the characteristic helix structure. Using these stacking interactions, this structure is implicitly imposed in the OxDNA model. This is in contrast with the traditional approach, used in coarse grained-models like Martini[,] en 3SPN[,], where the double helix structure is explicitly constructed. This implicit structure allows for the unstacking of nucleotides, which especially in ssDNA is an important contribution to the flexibility of the strand.

During the simulations of the DNA nanopiston, both the flexibility of the ssDNA strands and the DNA thermodynamics play an important role. Since both aspect of DNA are accurately captured by the OxDNA model, it provides a logical choice for our simulations. The low number of degrees of freedom in the model allows us to study computationally intensive simulations like DNA thermodynamics.

3.2 DNA Thermodynamics

The field of DNA thermodynamics focuses on understanding how the structure of DNA varies with temperature. Due to the nature of hydrogen bond interactions, that give rise to the structure of dsDNA, the association and dissociation of the DNA duplex is possible. The former is called DNA hybridisation shown in fig. ..., driven by a reduction in free energy due to the bonding of complementary base-pairs. The latter is called DNA melting, a process observed at high temperatures. This dissociation is energetically driven, since the reduction in free energy due to base-pair hybridisation is no longer a favourable trade-off with the reduction in configurational entropy in the duplex structure.

During the discussion of the DNA nanopiston, we stated that thermodynamic transitions of DNA are the driving force behind its operating cycle. The power stroke of the piston is induced by a toehold mediated strand displacement reaction, while a hybridisation reaction facilitates the recovery stroke.

Initiating a hybridisation reaction between two strands of ssDNA incurs a thermodynamic penalty. This penalty originates in the decrease of configurational entropy, when the strands start to form a duplex. This has a consequence that initial contacts in these reactions often dissociate, due to the initial energy barrier that needs to be crossed before the full hybridisation becomes energetically favourable. Even when an initial contact results in the stabilisation of a dsDNA duplex for select base-pairs, the configuration often times is not conducive to full duplex formation. Especially in repetitive sequences, the chance of a mismatched initial hybridisation is significant.

Another limiting factor to the rate constant of hybridisation reactions is that these transitions are not characterised by a single state, but rather by an ensemble of possible transition pathways. The number of pathways increase dramatically when the strand sequences are repetitive, giving rise to hybridisation pathways facilitated by Inchworm and pseudo-knot displacements[.].

The combination of the unstable initialisation of hybridisation reactions together with its many transition pathways, complicates the analysis of the full reaction kinetics observed in DNA hybridisation.

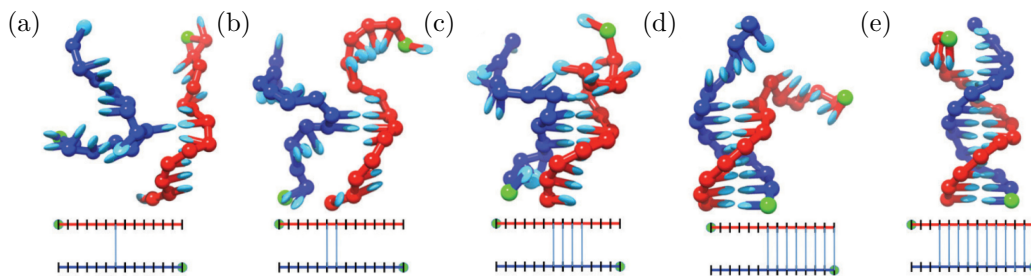


Figure 3.2: This is a figure [.]

The other important thermodynamic transition in the operating cycle of the nanopiston is a toehold mediated strand displacement. Initially this reaction consists out of two components. The first is an imperfect duplex structure, formed by a substrate strand and an incumbent strand. The two strands are partially complementary by having either a mismatch in their base-pair sequence or a surplus of base-pairs on the substrate strand. The non-hybridised part of the substrate constitutes a flexible strand of ssDNA that is referred to as the toehold.

The second component is called the invasive strand, and is fully complementary with the substrate. It is energetically favourable for the invading strand to disrupt the imperfect duplex structure and form a fully WatsonCrick complementary dsDNA with the substrate strand. This displacement reaction results in an overall reduction in the free energy of the system, since the strand displacement increases the total number of hybridised base-pairs.

The process of strand displacement starts with the hybridisation of the toehold and the invading strand. Once this initial hybridisation has occurred the invading strand can start to contest hybridised base-pairs of the imperfect duplex. Disrupting the base-pairing of the duplex is referred to as fraying, while the reverse process where new base-pairs are formed

3. IMPROVING THE MODEL

is called zippering. During this process the invading strand competes with the incumbent strand to form base-pairs with the substrate.

The reaction can be modelled using an one-dimensional energy landscape, called the intuitive energy landscape (IEL) model[.], shown in figure In the shape of the energy landscape we recognise two distinct features. The first features is the initial energy barrier, also seen in DNA hybridisation. This energy barrier again arises from a reduction in configurational entropy, when the initial binding happens. The second feature is the plateau, representing the change in free energy when the strand displacement takes place. This plateau gives rise to a relatively slow reaction, which can be explained using a simple toy model. Considering a scenario, where the substrate consists of $N + 1$ nucleotide, with only one of these nucleotides constituting the toehold. If we now assume that both the incumbent and invasive strand contest each others hybridised base-pairs at the same rate, the displacement reaction can be modelled as a random walk. The model is reduced to a famous problem in probability theory, called the gamblers ruin. It can be shown that the reaction rate scales as $1/3N[.]$, making the Toehold displacement reaction increasingly difficult to study for large strands.

These two types of thermodynamic transitions, central in the operation cycle of the DNA nanopiston, are relatively difficult to study due to their slow reaction rates and initial energy barrier. Accurately analysing the reaction kinetics of these rare events, requires the use of advanced sampling techniques.

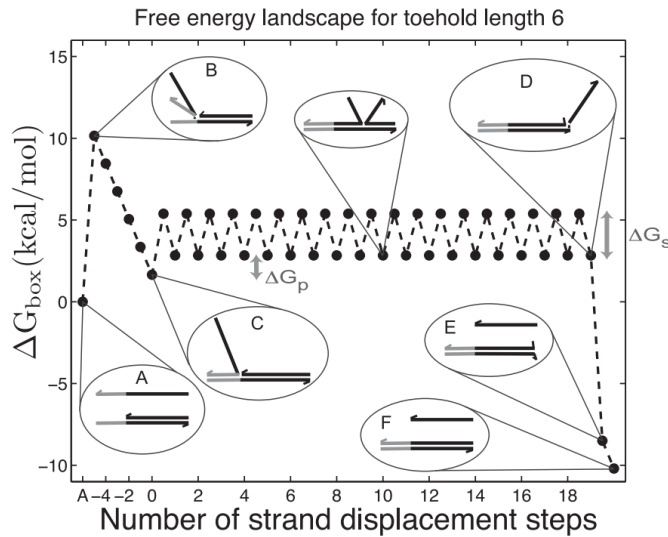


Figure 3.3: write caption[.]

3.3 Forward Flux sampling

Computational methods are used to study a wide variety of phenomena, ranging from large meteorological events to chemical reactions at the atomic scale. One class of phenomena that is omnipresent in all these fields are the rare events. A rare event is an event caused by stochastic fluctuations in the system, characterised by a large difference in the time-scales corresponding to the duration of the events and their temporal spacing. The infrequency of their occurrence in combination with their short duration, makes them hard to study with both experimental and computational approaches.

Using this definition, the hybridisation and toehold displacement reactions studied in this thesis can be classified as a rare event. Due to the large temporal spacing of these rare events, simulating them with a brute-force approach is inefficient. In this case, molecular dynamics simulations spend a lot of computational resources on simulating the waiting time between events. To effectively probe the kinetics of these rare events, advanced sampling methods are needed.

A large ensemble of advanced sampling methods have been developed and can be largely divided into two classes. The first class encompasses the free energy methods, based upon applying a biasing potential onto chosen collective variables. These potentials bias the Hamiltonian of the system in such a way, that rare parts of its configurational space are explored. Notable examples of these methods are the adaptive biasing force algorithm[.], basis function sampling[.] and umbrella sampling[.].

The second class of methods, known as path sampling methods, do not influence the systems Hamiltonian, but rather interface directly with the simulated trajectories. The transition path ensemble is usually sampled by perturbing an initial transition path or partitioning the phase space in subregions. Examples of these methods are transition path sampling[.] and forward flux sampling[.][.]. The latter will be used in our hybridisation simulations, motivated by its relative simplicity.

Forward Flux Sampling (FFS) starts with identifying two local minima, A and B , in the energy landscape of our system, for which we want to sample the transition path ensemble. Next an order parameter, $\lambda(x)$, is defined with the aim of partitioning the phase space, Ω , using a set of nonintersecting hypersurfaces. By design, we choose this order parameter to be a function, $\lambda(.) : \Omega \rightarrow \mathcal{R}$, monotonically increasing from the initial state A to the final state B .

Using this function the two local minima can now be specified as $A := \{x : \lambda(x) < \lambda_A\}$ and $B := \{x : \lambda(x) \geq \lambda_B\}$. The chosen levels of order, λ_A and λ_B , construct the interfaces separating the two local energy basins from the rest of the phase space. Finally, this procedure can be done for a N -number of interfaces partitioning the space between A and B , for which we require

$$\lambda_A = \lambda_0 < \lambda_1 < \dots < \lambda_{N-1} < \lambda_N = \lambda_B. \quad (3.2)$$

Note that this method does not require an in depth knowledge of the systems energy landscape, however the choice of order parameter will heavily influence the efficiency of the

3. IMPROVING THE MODEL

simulation. Analogous to the ambiguous choice of a collective variable in free energy methods, constructing these hypersurfaces is often more an art than a science.

The ultimate aim of these methods is to get a grasp of the kinetics of rare events. In quantitative terms this means determining the rate constant of the transition from A to B , denoted as k_{AB} . The expression used to calculate k_{AB} is:

$$k_{AB} = \frac{\langle \Phi_{A,n} \rangle}{\langle h_A \rangle} = \frac{\langle \Phi_{A,0} \rangle}{\langle h_A \rangle} P(\lambda_n | \lambda_0), \quad (3.3)$$

where $\langle \Phi_{A,n} \rangle$ is the steady-state flux of trajectories starting in A and reaching the final interface λ_n (i.e. reaching B) and $\langle h_A \rangle$ is the average fraction of time that a trajectory spends in the basin of local minima A . In the above equation this steady state flux is factorised into the flux of trajectories starting in A and crossing λ_0 and the subsequent probability of reaching the final state from this interface. Using the previously defined interfaces, we can now factorise the events' probability into transition probabilities between the individual interfaces as

$$P(\lambda_n | \lambda_0) = \prod_{i=0}^{n-1} P(\lambda_{i+1} | \lambda_i). \quad (3.4)$$

Estimating these transition probabilities can be done by shooting trajectories starting from one interface to the next, while keeping track of the fraction of attempts successfully crossing the next interface. Since not the entire energy landscape between the minima has to be crossed, measuring these small transitions can be more easily done.

Note that this set-up allows for simulations of both equilibrium and out-of-equilibrium systems, since it does not require detailed balance like other sampling techniques. Non-equilibrium systems are ubiquitous in soft matter physics, illustrating another strength of the method. Different variants on the FFS method have been devised, differing in the approach

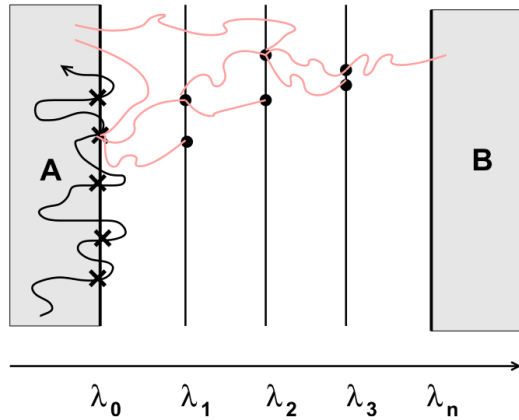


Figure 3.4: write caption[.]

by which they calculate the probability $P(\lambda_n | \lambda_0)$. During this thesis I chose to use the

Rosenbluth-like (RB) method [zie citation allen review]. The choice is motivated by its resemblance with well known Monte Carlo Simulations and recursive nature, making it easy to implement. This method generates unbranched transition paths from state A to state B , making them easy to analyse. The algorithm is described in six steps:

- (i) Generate configurations on the λ_0 interface by running simulations in the A basin. Keeping track of the fraction of successful runs, $\langle \Phi_{A,0} \rangle / \langle h_A \rangle$ is evaluated.
- (ii) Fire k_0 trial runs from generated configurations on λ_0 until they cross λ_1 or cross back to λ_0 . Store the final configurations of the successful simulations.
- (iii) Sample one of the saved configuration on the λ_1 interface and use it to shoot k_1 runs to the next interface λ_2 .
- (iv) Iterate the previous steps until the trajectories reach λ_n or no more configurations are available.
- (v) If not successful, sample a stored configuration on λ_0 and repeat the steps (i) to (iv).
- (vi) Finally compute $P(\lambda_n | \lambda_0)$ using a weighted average of individual transition probabilities as described below.

Calculating the transition probabilities is done by taking a weighted average of the attempted trial runs. The path b starting at the initial basin and reaching interface λ_i is assigned a weight $w_{i,b}$ as

$$w_{i,b} = \prod_{j=0}^{i-1} S_{j,b} / k_j, \quad (3.5)$$

where $S_{j,b}$ is the number of successful trajectories crossing interface j during the generation of path b . Using these weights, the transition probability is computed using

$$P(\lambda_{i+1} | \lambda_i) = \frac{\sum_b w_{i,b} S_{i,b} / k_i}{\sum_b w_{i,b}}. \quad (3.6)$$

3.4 Computational setup

The model used to study the DNA nanopiston, is largely based on the model previously devised by Bayoumi et al. The main variation between the two models lays in the different coarse-grained models, used to simulate the DNA strands. As discussed in Chapter 2, the Bayoumi model uses a bead-spring approach to simulate DNA strands, where we use a more sophisticated model called oxDNA. This DNA model gives a better representation of the dynamics of DNA strands, at the same time allowing for accurate simulations of the thermodynamic transitions in the DNA nanopiston.

The simulations are performed using the popular molecular dynamics simulator, LAMMPS[.]. Employing the Lammps implementation of oxDNA developed by Henri et al[.], it becomes

3. IMPROVING THE MODEL

possible to study the interactions between oxDNA strands and externally defined particles. The initial configurations of the simulations are generated using the Moltemplate package[.], a general purpose molecule builder for LAMMPS.

The molecular dynamics simulations performed in this thesis utilises a langevin thermostat, more precisely the Dot-C langevin integrator also implemented by Henri et al. This is a LAMMPS implementation of the Langevin C integrator developed by Davidchack et al. [.], falling in the class of rigid-body Langevin-type integrators. This type of thermostat separates the stochastic and deterministic parts of a Langevin thermostat to efficiently take into account the extra degrees of freedom in the system, arising from the non-spherical shape of the oxDNA beads. As is common practice in MD simulations, the diffusion coefficient of the oxDNA strand is chosen larger then the value of physical DNA. This is done to speed up the simulations, while ensuring its physical accuracy.

The model is used to more accurately study the conformational fluctuations of the Rotaxane and develop understanding of the entropic interactions between the DNA and the nanopore. Next the thermodynamic transitions in the operation cycle of the piston are simulated using a forward flux sampling algorithm. The FFS algorithm is implemented as a Python script, performing the simulations by interfacing with the Python API of LAMMPS.

CHAPTER 4

Simulations of the Rotaxane

The career of a young theoretical physicist consists of treating the harmonic oscillator in ever-increasing levels of abstraction.

— Sidney Coleman

4.1 Mixed Rotaxane

To highlight the crucial role of the entropic forces, we designed and studied four different rotaxanes, hereby referred to as mixed rotaxanes. These are an alternative version of rotaxane-ds, in which the toehold is removed, and the ssDNA connection strand varied in length. the total length of the rotaxane thread was fixed at 100 nt/bp, with the ss-DNA connection strand length varying from 0 nt to 40 nt and the ds DNA varying from 100 bp to 60 bp, in steps of 10 nt/bp

We then performed I-V measurements in the range, see figure.

The mixed rotaxane composed entirely of dsDNA yields an almost linear I-V plot in the measured voltage range indicating a constant obstruction of the nanopore. constant resistance of the nanopore.

The rotaxane with a 10 nt ssDNA, however, has a rather different behavior. Observed blockage at high voltages in experiments.

Longer strands we observe no blockage.

Shed light on these experimental results we performed MD Simulations at zero bias, here the entropic contributions can be isolated.

1D diffusion

We identify the z-axis with the symmetry axis of the pore and fix the origin of the coordinate system at the center of the trans-entry of the pore. The center of the cis entry is

4. SIMULATIONS OF THE ROTAXANE

then located at $r_{cis} = (0, 0, z_0)$, with respect to the origin, where $z_0 = 14.3 \text{ nm}$ (see Figure S6). We define the reaction coordinate as follows

$$X = \begin{cases} Z_0 + |\mathbf{r} - \mathbf{r}_{cis}|, & \text{if on cis-side} \\ Z, & \text{if inside pore} \\ -|\mathbf{r}|, & \text{if on trans-side} \end{cases} \quad (4.1)$$

The simulation data show that the peak gradually shifts towards negative values of X with increasing ssDNA length, suggesting that full pore blockage requires increasingly stronger electrophoretic force.

4.2 Conformational Fluctuations of the Rotaxane

Electrophoretic, electro-osmotic and entropic forces are, in principle, acting on the rotaxanes. The electrophoretic force sets the negatively charged DNA in motion, under the action of the applied bias (from cis to trans for $\Delta V > 0$). Electroosmosis generates an opposing force, arising from the motion of cations accumulated on the walls of the negatively charged ClyA pore and the DNA thread. Finally, the entropic force is solely geometry specific, and pushes the rotaxane towards conformations with high configurational entropy

Entropic forces are expected to play an important role in the rotaxanes studied here, which are composed of stiff dsDNA and flexible ssDNA parts.

Rarely the toehold is captured inside the nanopore. Occurs more often when the applied voltage induces an upward force on the rotaxane. This process is important in explaining why the cycles are faster at positive than at negative applied potentials, but were slower as the potential was increased.

To gain some insight on these entropic forces, we performed computer simulations of the rotaxane/ClyA complex in absence of an applied potential ($\Delta V = 0$)

We identify the z-axis with the symmetry axis of the pore and fix the origin of the coordinate system at the center of the trans-entry of the pore. The center of the cis entry is then located at $r_{cis} = (0, 0, z_0)$, with respect to the origin, where $z_0 = 14.3 \text{ nm}$ (see Figure S6). We define the reaction coordinate as follows

$$X = \begin{cases} Z_0 + |\mathbf{r} - \mathbf{r}_{cis}|, & \text{if on cis-side} \\ Z, & \text{if inside pore} \\ -|\mathbf{r}|, & \text{if on trans-side} \end{cases} \quad (4.2)$$

4.3 Toehold Displacement Reaction

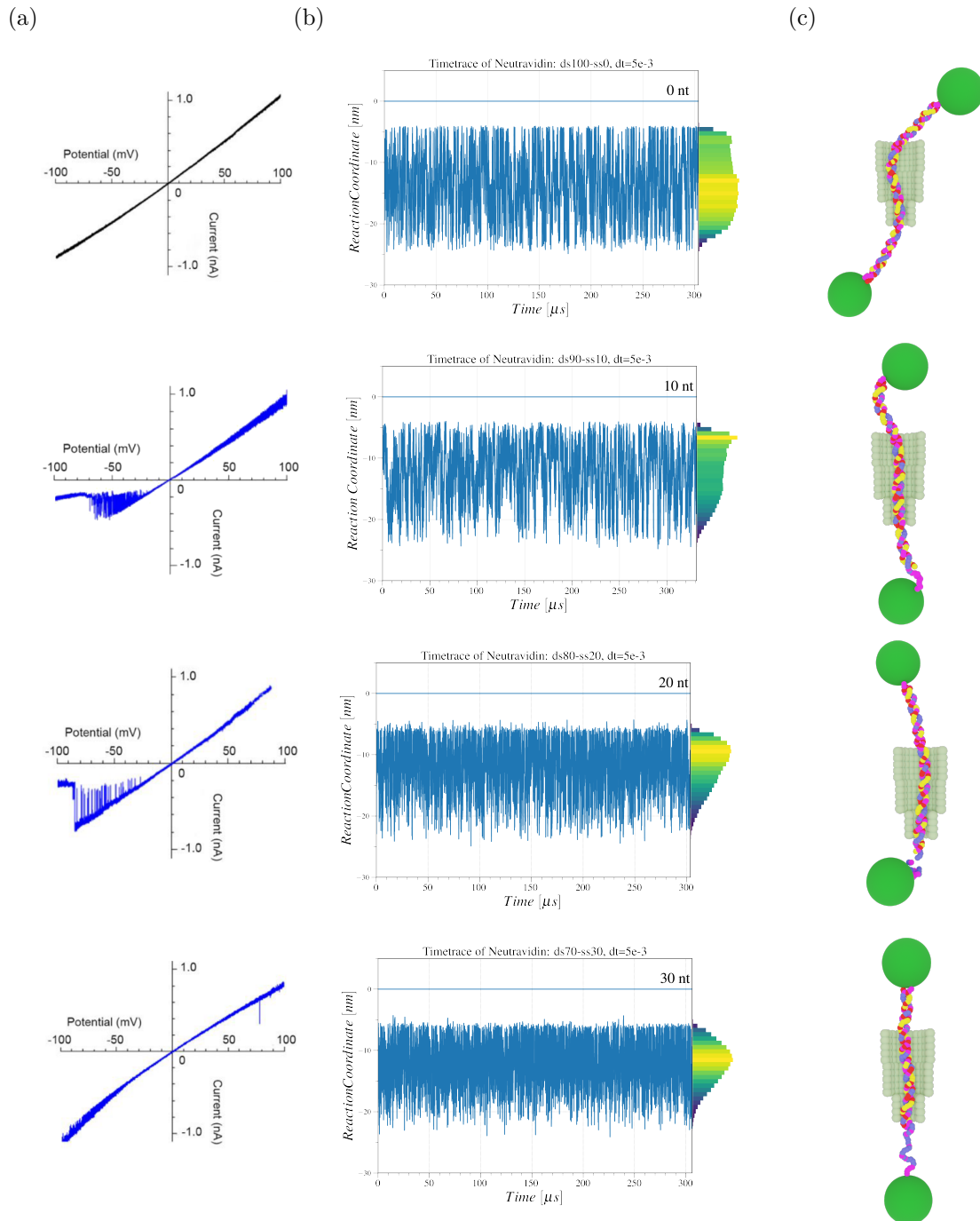


Figure 4.1: asdf asdf asdf asdf asdf asd fasd fasdf asf asdfasdf asdfasdf asfasf. asdf asdf asdf asdf asd fasd fasdf asf asdfasdfa asdfasdf asfasf. asdf asdf asdf asdf asd fasd fasdf asf asdfasdfa asdfasdf asfasf. asdf asdf asdf asdf asd fasd fasdf asf asdfasdfa asdfasdf asfasf.

4. SIMULATIONS OF THE ROTAXANE

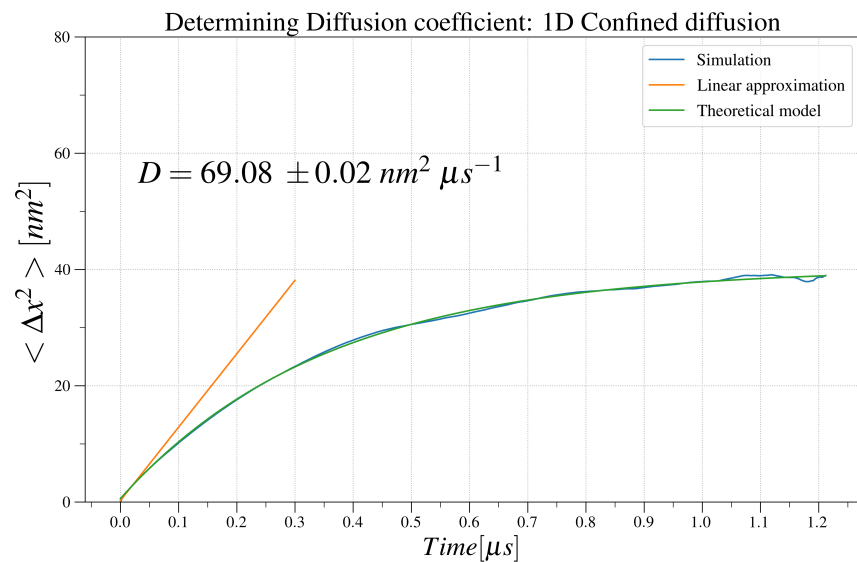


Figure 4.2: write caption

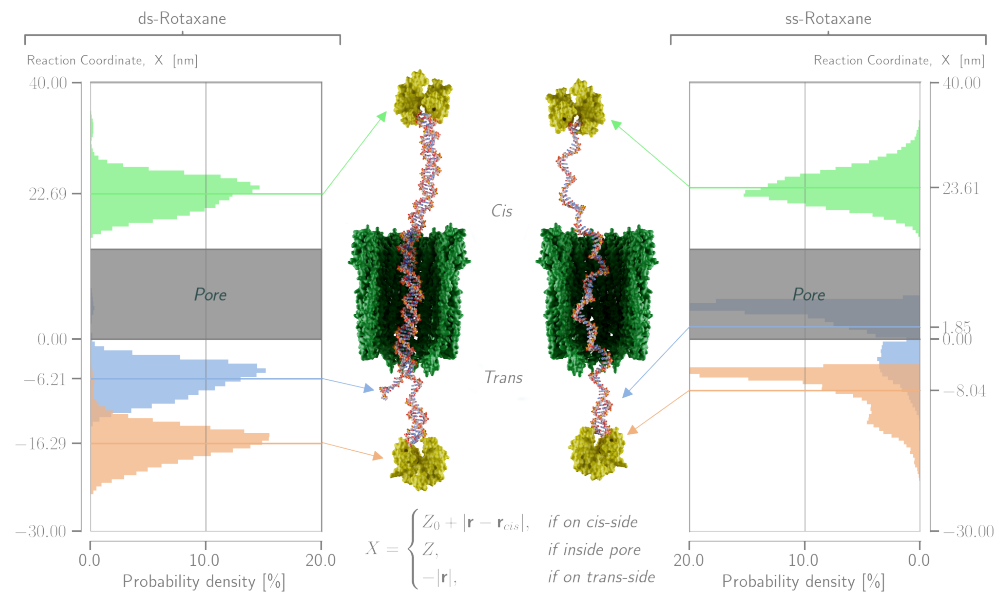


Figure 4.3: write caption

CHAPTER

5

Conclusions and Perspectives

All models are wrong, but some are useful.

— George Box

5.1 Results & Conclusions

5.2 Future Perspectives

APPENDIX A

1D Confined Diffusion

Studying the dynamics of the mixed rotaxane highlighted the importance of entropic interactions between the nano pore and the DNA strand. Here we observed that a fully double stranded DNA polymer represented a special case. The uniformity of the \mathcal{X} histogram corresponding to this 0 nt mixed rotaxane suggests a free diffusive motion of the rotaxane in a bounded one-dimensional domain. This isotropic behaviour was previously also observed in the bead-spring simulations by Bayoumi et al.¹

$$\langle \Delta x^2 \rangle \simeq 2nDt.$$

$$\frac{\partial \psi}{\partial t} = D \frac{\partial^2 \psi}{\partial x^2}, \quad \psi(x, t) = f(x)g(t)$$

Reflecting boundary conditions $j = -D \frac{\partial \psi}{\partial x} = 0$. Current vanishes at the boundaries

$$t : \quad \dot{g} = -\alpha g(t) \Rightarrow g(t) = e^{-\alpha t}$$

$$\begin{aligned} x : \quad D \ddot{f} = -\alpha f(x) &\Rightarrow f(x) = A \sin(Kx) + B \cos(Kx) \\ &= B \cos\left(\frac{\pi n x}{L}\right) \end{aligned}$$

$$\frac{\alpha}{D} = \frac{\pi^2 n^2}{L^2}$$

The general solution is given by the linear combination,

$$\begin{aligned}\psi(x, t) &= \sum_{n=0}^{+\infty} C_n \cos\left(\frac{\pi n x}{L}\right) e^{-\frac{D\pi^2 n^2}{L^2} t} \\ &= \frac{1}{L} \left[1 + \sum_{n=1}^{+\infty} \cos\left(\frac{\pi n x_0}{L}\right) \cos\left(\frac{\pi n x}{L}\right) e^{-\frac{D\pi^2 n^2}{L^2} t} \right] \\ \langle \Delta x^2 \rangle &= \langle (x - x_0)^2 \rangle \\ &= \frac{L^2}{6} \left[1 - \frac{96}{\pi^4} \sum_{k=0}^{+\infty} \frac{1}{(2k+1)^4} e^{-\frac{D(2k+1)^2 \pi^2}{L^2} t} \right]\end{aligned}$$

As expected, the mean squared distances saturates to $\langle \Delta x^2 \rangle = L^2/6$ in the long-time limit $t \gg L^2/D$. To explore the other limiting case $t \ll L^2/D$ we perform a Taylor expansion and find

$$\langle \Delta x^2 \rangle = \frac{L^2}{6} - \frac{16L^2}{\pi^4} \sum_{k=0}^{\infty} \frac{1}{(2k+1)^4} + \frac{16Dt}{\pi^2} \sum_{k=0}^{\infty} \frac{1}{(2k+1)^2} + \mathcal{O}\left(\frac{D^2 t^2}{L^4}\right).$$

[cite in bickel]

$$\sum_{k=0}^{\infty} \frac{1}{(2k+1)^2} = \frac{\pi^2}{8} \quad \text{and} \quad \sum_{k=0}^{\infty} \frac{1}{(2k+1)^4} = \frac{\pi^4}{96}$$

$$\langle \Delta x^2 \rangle = 2Dt \quad t \ll L^2/D$$

Bibliography

- [1] Bayoumi, M., Nomidis, S. K., Willems, K., Carlon, E., and Maglia, G. (2021). Autonomous and active transport operated by an entropic dna piston. *Nano Letters*, 21(1):762–768. PMID: 33342212.
- [2] Feynman, Richard P. (Richard Phillips), .-. (c1963). *The Feynman lectures on physics*. Reading, Mass. : Addison-Wesley Pub. Co., c1963-1965. Vol. 2 has subtitle: The electromagnetic field; 3 has subtitle: Quantum mechanics.;Includes bibliographical references and indexes.

Acknowledgements

...

